RESOURCE

nature neuroscience

The microglial sensome revealed by direct RNA sequencing

Suzanne E Hickman[1], Nathan D Kingery[1], Toshiro K Ohsumi[2,3], Mark L Borowsky[2,3], Li-chong Wang[4], Terry K Means[1] & Joseph El Khoury[1,5]

Microglia, the principal neuroimmune sentinels of the brain, continuously sense changes in their environment and respond to invading pathogens, toxins and cellular debris. Microglia exhibit plasticity and can assume neurotoxic or neuroprotective priming states that determine their responses to danger. We used direct RNA sequencing, without amplification or cDNA synthesis, to determine the quantitative transcriptomes of microglia of healthy adult and aged mice. We validated our findings using fluorescence dual *in situ* hybridization, unbiased proteomic analysis and quantitative PCR. We found that microglia have a distinct transcriptomic signature and express a unique cluster of transcripts encoding proteins for sensing endogenous ligands and microbes that we refer to as the sensome. With aging, sensome transcripts for endogenous ligand recognition were downregulated, whereas those involved in microbe recognition and host defense were upregulated. In addition, aging was associated with an overall increase in the expression of microglial genes involved in neuroprotection.

Microglia, the principal resident immune cells of the brain, constitute 5–12% of brain cells depending on the region studied[1]. They are important in homeostatic functions in the brain, in host defense against infectious pathogens and in neurodegenerative diseases and traumatic brain injury[2]. The role of microglia as mononuclear phagocytes has been recognized for decades and their involvement in inflammatory and necrotizing processes are beginning to be elucidated[3].

In the past decade, we have witnessed an explosion of research into understanding the role of microglia in the developing, healthy, aging and diseased brain. Seminal work showed that a major function of these cells is to constantly survey their environment sensing any changes in that environment and responding to them[4]. The genes that encode the microglial sensing apparatus are not defined.

Microglia, as with other mononuclear phagocytes, including macrophages, exhibit plasticity and can assume neuroprotective or neurotoxic phenotypes[5–7]. In advanced stages of neurodegenerative disorders such as Alzheimer's disease, multiple sclerosis and amyotrophic lateral sclerosis, microglia become neurotoxic[7–9]. Microglia also exhibit various priming states that determine their responses to subsequent injury or infection of the brain. Two of these priming states include the classical priming state which occurs in response to stimulation with interferon-γ, and the alternative priming state associated with exposure of these cells to interleukin (IL) 4 or IL13 (refs. 8,10,11). Classically primed mononuclear phagocytes are neurotoxic, whereas alternatively primed cells promote axonal elongation and sprouting and are considered to be neuroprotective[8,12].

Aging markedly affects the gene expression profile of the brain[13]. Transcriptome profiling of the whole brain using microarrays found downregulation of genes involved in energy production, protein synthesis and protein transport with aging and upregulation of many genes that regulate proliferation[14]. Studies looking at aging-associated changes in individual cells have been limited[15] and quantitative changes that occur in the microglial transcriptome with aging have not been defined.

Several approaches to analyze the transcriptomes of tissues and cells have been developed. These include quantitative PCR (qPCR)[16], microarrays[17,18], Nanostring[19] technology and deep sequencing (RNA-Seq)[20]. Valuable information can be obtained from each of these approaches. Although qPCR and Nanostring are quantitative, they are limited by the number of transcripts that can be measured. Microarrays are very useful, but only provide a semiquantitative assessment of the transcriptome. Available RNA-Seq platforms are quantitative and provide a snapshot of the transcriptome of cells at a specific time point, but vary in their requirements of the amount of RNA as a starting material and require generation of cDNA and amplification if the sample size is small[21]. Because the number of microglia that can be harvested is limited, we were interested in an approach that utilizes small amounts of RNA, does not require cDNA synthesis or amplification, and yields robust quantitative results.

To analyze the transcriptome of microglia, we selected a recently developed technology, direct RNA sequencing (DRS), because it allows for the quantification of mRNA without the need for amplification or cDNA synthesis[22], thereby providing several advantages

[1]Center for Immunology and Inflammatory Diseases, Massachusetts General Hospital, Charlestown, Massachusetts, USA. [2]Department of Molecular Biology, Massachusetts General Hospital, Charlestown, Massachusetts, USA. [3]Department of Genetics, Harvard Medical School, Boston, Massachusetts, USA. [4]Advanced Cell Diagnostics, Hayward, California, USA. [5]Division of Infectious Diseases, Massachusetts General Hospital, Charlestown, Massachusetts, USA. Correspondence should be addressed to S.E.H. (shickman@partners.org) or J.E.K. (jelkhoury@partners.org).

Received 3 June; accepted 17 September; published online 27 October 2013; doi:10.1038/nn.3554

over existing techniques. Essentially, poly(A) mRNA is hybridized to a surface coated with poly(dT), unbound RNA (non-mRNA) is washed away and the remainder of the poly(A) tail is blocked, followed by sequencing (Online Methods). Using this approach, we determined the unbiased quantitative transcriptome of microglia isolated from adult 5-month-old mice and compared it with that of peritoneal macrophages isolated from the same mice and with that from whole brain. The data sets that we generated allowed us to identify a cluster of genes that constitute the microglia sensing apparatus, which we refer to as the sensome. We also identified a unique microglial signature that distinguishes them from macrophages. Furthermore, we determined changes that occur in the microglial transcriptome and sensome during normal aging using microglia isolated from 24-month-old mice. With aging, the microglial overall gene expression profile revealed an upregulation of genes involved in host defense and neuroprotection. To the best of our knowledge, our data set provides the first quantitative transcriptome of normal microglia in adulthood and aging.

RESULTS

We used C57BL/6 mice obtained from the National Institute of Aging mouse colony as a standardized source of cells. Microglia were isolated from 5-month-old adult mice by enzymatic digestion, as previously described[7], and peritoneal macrophages were isolated by peritoneal lavage[23]. Cells were stained with fluorescent antibodies to CD11b and CD45, two well-established microglia and macrophage markers[2,24] (**Supplementary Fig. 1a**). Microglia and macrophages were subsequently isolated by fluorescence activated cell sorting (FACS) and RNA was extracted (**Supplementary Fig. 1b**,**c**).

Identification of the microglial sensome by DRS

We performed DRS on RNA isolated from whole brain (three samples from two mice each) and microglia isolated from three pools comprising 22, 10 and 20 mice. We developed programs in MolBioLib to annotate the various sequences obtained[25] and then analyzed the data using gene set enrichment analysis (GSEA)[26] and edgeR[27]. A total of 21,025 different coding transcripts were detected (**Supplementary Fig. 1d**). To standardize data presentation and allow for comparison between different data sets, we computed the data for each transcript as copies of mRNA per million mapped reads (CMMR).

Microglia processes constantly move in the area surrounding the cell body, sensing any changes in the environment[4]. Such changes could be caused by microbial invasion, cell injury or death associated with neurodegeneration, deposition of neurotoxic substances such as amyloid β[23,28], or inflammatory molecules such as chemokines and cytokines. Additional milieu alterations could include changes in pH, the composition or integrity of the extracellular matrix, or extracellular metabolites such as nucleotides or amino acids. A large armamentarium of proteins and receptors may be used by a given cell for sensing such changes in the environment. The full spectrum of the cellular receptors and proteins used by microglia for this purpose are not known. Here, we define these proteins as the sensome of microglia.

We used the DAVID[29] Gene Ontology (GO) analysis software as well as manual

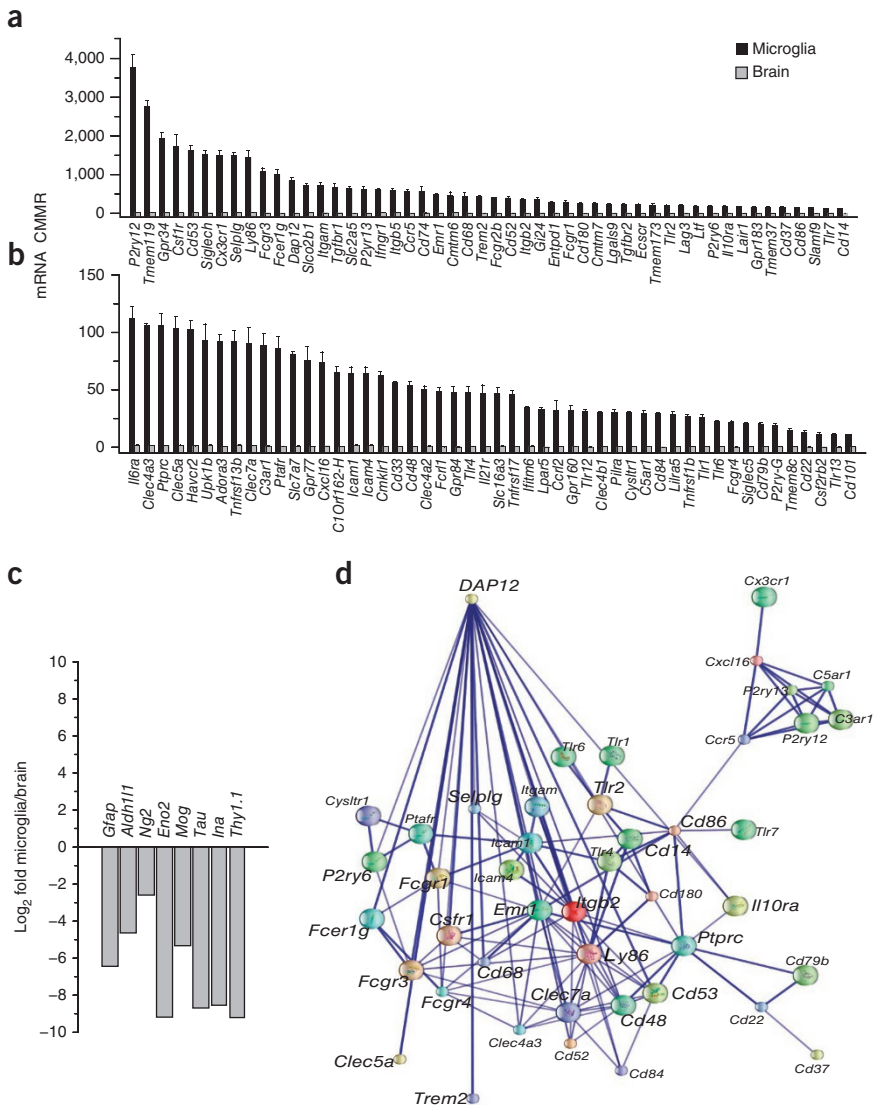

Figure 1 The microglial sensome identified by direct RNA sequencing. Of the 21,025 transcripts measured, we used gene ontology (GO) analysis and identified 1,299 potential sensome genes. Of these, we selected the top 100 transcripts with the highest enrichment of microglia versus brain and termed this gene collection the microglial sensome. (**a**,**b**) Expression levels of genes of the microglial sensome in mRNA CMMR in microglia and brain. Values represent the mean ± s.d. of three different experiments carried out with microglia pooled from 22, 10 and 20 mice and three pools of RNA from two brains each. $P < 0.00001$ for differences in expression between microglia and brain for all sensome genes shown (also see **Supplementary Table 1**). (**c**) Log_2 fold change (gray bars) of microglia/brain genes specific for neurons, astrocytes and oligodendrocytes show 'derichment' in microglia compared to whole brain. (**d**) Network analysis of the microglial sensome by STRING identified a DAP12-centered pathway, with 44 of 100 genes directly or indirectly interacting with DAP12. Of these, 24 had a direct interaction with Dap12, and are indicated using a larger font.

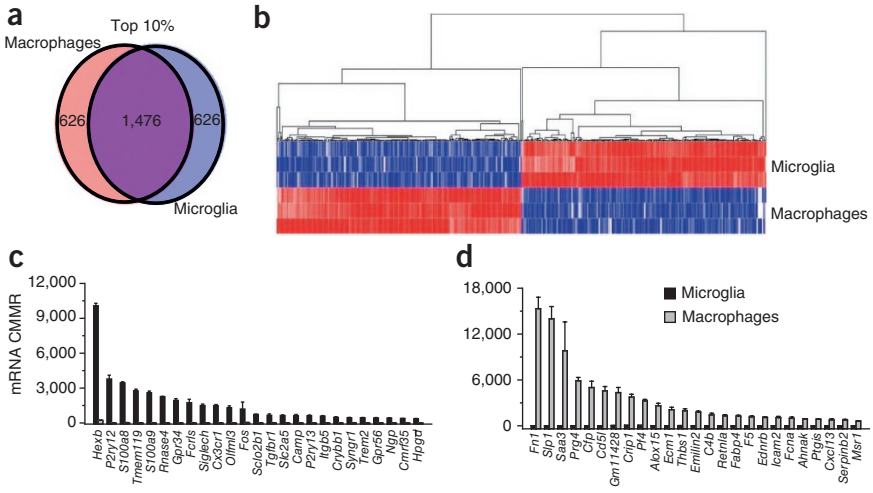

Figure 2 Differences between microglia and macrophages revealed by DRS. (**a**) Venn diagram showing similarities and differences of the top 10% of transcripts expressed in microglia and macrophages. (**b**) Heat map and hierarchal clustering of the transcripts that are unique to microglia or macrophages, showing a distinct signature for each of the cell types. (**c**) The top 25 transcripts with the highest CMMR that were unique to microglia were barely detectable in macrophages ($P < 0.00001$ for differences between microglia and macrophage expression). These 25 transcripts showed a high level of enrichment ($\log_2$ fold change >4) over macrophages regardless of the level of expression in microglia. (**d**) The top 25 transcripts unique to macrophages with the highest CMMR had barely detectable levels in microglia ($P < 0.00001$ for differences between macrophages and microglia expression). These 25 transcripts showed high levels of enrichment ($\log_2$ fold change >5) over microglia regardless of the level of expression in macrophages. Values in **c** and **d** are presented as mean ± s.d. of three different experiments carried out with microglia pooled from 22, 10 and 20 mice, and three pools of macrophages from ten mice per pool (see **Supplementary Table 2**).

annotation and data mining in PubMed (http://www.ncbi.nlm.nih.gov/pubmed) to identify candidate sensome genes, regardless of their level of expression. These potential sensome genes included all transmembrane proteins and receptors, such as integrins, purinoceptors, lectins, transporters and CD antigens, but not genes encoding secreted proteins or proteins expressed only in nuclear, mitochondrial or endoplasmic reticulum membranes. This analysis identified 1,299 candidate sensome genes.

To identify the transcripts that are highly enriched in microglia versus whole brain, we computed the ratio $E = \frac{\text{CMMR(microglia)}}{\text{CMMR(brain)}}$, calculated $\log_2 E$ values and selected the 100 transcripts with the highest E values. These transcripts are the ones most likely to be microglia specific (**Fig. 1a**,**b** and **Supplementary Table 1**). The E value for these transcripts ranged from 36 to 292. Of these transcripts, 46% had an E value ≥ 100, indicating a high level of enrichment in microglia ($P < 0.00001$; **Fig. 1a**,**b** and **Supplementary Table 1**). In contrast, the E values for neuronal genes, such as gamma enolase (neuron-specific enolase *Eno2*), internexin (*Ina*) and *Thy1*, were 0.0018, 0.0028 and 0.0018, respectively. Similarly, the E values for the oligodendrocyte genes myelin-oligodendrocyte glycoprotein (*Mog*) and chondroitin sulfate proteoglycan 4 (*Cspg4*) were 0.026 and 0.17, respectively. Furthermore, the E values for the astrocyte markers glial fibrillary acidic protein (*Gfap*) and aldehyde dehydrogenase family 1 member L1 (*Aldh1l1*) were 0.012 and 0.042, respectively (**Fig. 1c**). These data indicate a high level of enrichment of microglia specific sensome genes and a 'derichment' of genes expressed by neurons and other non-microglial cells of the neural environment in our purified microglia.

We used gene ontology analysis to classify the sensome transcripts into pattern recognition receptors (25%), chemoattractant and chemokine receptors (10%), Fc receptors (7%), purinergic receptors (8%), receptors for extracellular matrix (ECM) proteins (6%), cytokine receptors (10%), receptors involved in cell-cell interaction (10%), other receptors or transporters (13%), and potential sensome proteins with no known ligands (11%) (**Supplementary Fig. 1e** and **Supplementary Table 1**). We expected some of the receptors that we identified, as microglia have macrophage-like functions. These included *Cd11b*, *Cd14*, *Cd68*, *Tlr2* and *Tlr7*, *Cxcl16*, various Fc receptors, and others. Notably, 32% of transcripts of the microglial sensome that we identified have not been described in microglia, including *Entpd1*, *Tgfbr2*, *Cmtm7*, *Ly86*, *Cd180*, *Slco2b1*, *Gi24* and *Clec4a2* (**Supplementary Table 1**).

These data comprehensively identify the armamentarium of genes used by microglia to sense their environment. The diversity of the ligands recognized by the surface proteins encoded by these genes provides strong evidence that supports a broad role for microglia in homeostasis, host defense and response to injury. Of note, two of these sensome genes, *Trem2* and *Cd33*, were recently identified as risk factors for Alzheimer's disease[30–33], further attesting to the importance and relevance of our data.

To identify known and potential protein-protein interactions relevant to the sensome, we used the STRING 9.1 software and database[34]. STRING quantitatively integrates protein interaction data from multiple sources for a large number of organisms, and transfers information between these organisms where applicable. The database currently covers 5,214,234 proteins from 1,133 organisms. Using STRING, we found that 44 of 100 sensome proteins had a direct or indirect association with DAP12, an adaptor that regulates signaling via TREM2 (ref. 35). Of these, 24 proteins appeared to have direct association with DAP12 (**Fig. 1d**). These proteins are Trem2, P2ry6, Fcer1g, Fcgr3, Fcgr1, Fcgr4, Clec4a3, Clec5a, Clec7a, Selplg, Csf1r, Cd14, Cd48, Cd52, Cd53, Cd68, Cd84, Cd86, Ly86, Itgb2, Tlr2, Ptprc, Emr1 and Il10ra. These data indicate that DAP12 may be an important regulator of the microglial sensing function through direct and indirect interaction with other sensome proteins.

Microglia versus macrophages

Both microglia and macrophages are resident tissue mononuclear phagocytes and share several functions, including phagocytosis, production of reactive oxygen and nitrogen species, and response to chemokines and purinergic stimuli[36]. To identify similarities and differences between resting microglia and macrophages, we used DRS to compare the transcriptome of peritoneal macrophages with that of microglia isolated from the same mice (see Online Methods). We compared the top 10% of transcripts with the highest expression in macrophages with those of microglia (**Fig. 2a**). Of these 2,102 transcripts, microglia and macrophages shared 1,476 transcripts, suggesting a substantial number of similarities between the two cell types (**Fig. 2a**). Microglia and macrophages, however, also had substantial differences in their transcriptomes and each expressed 626

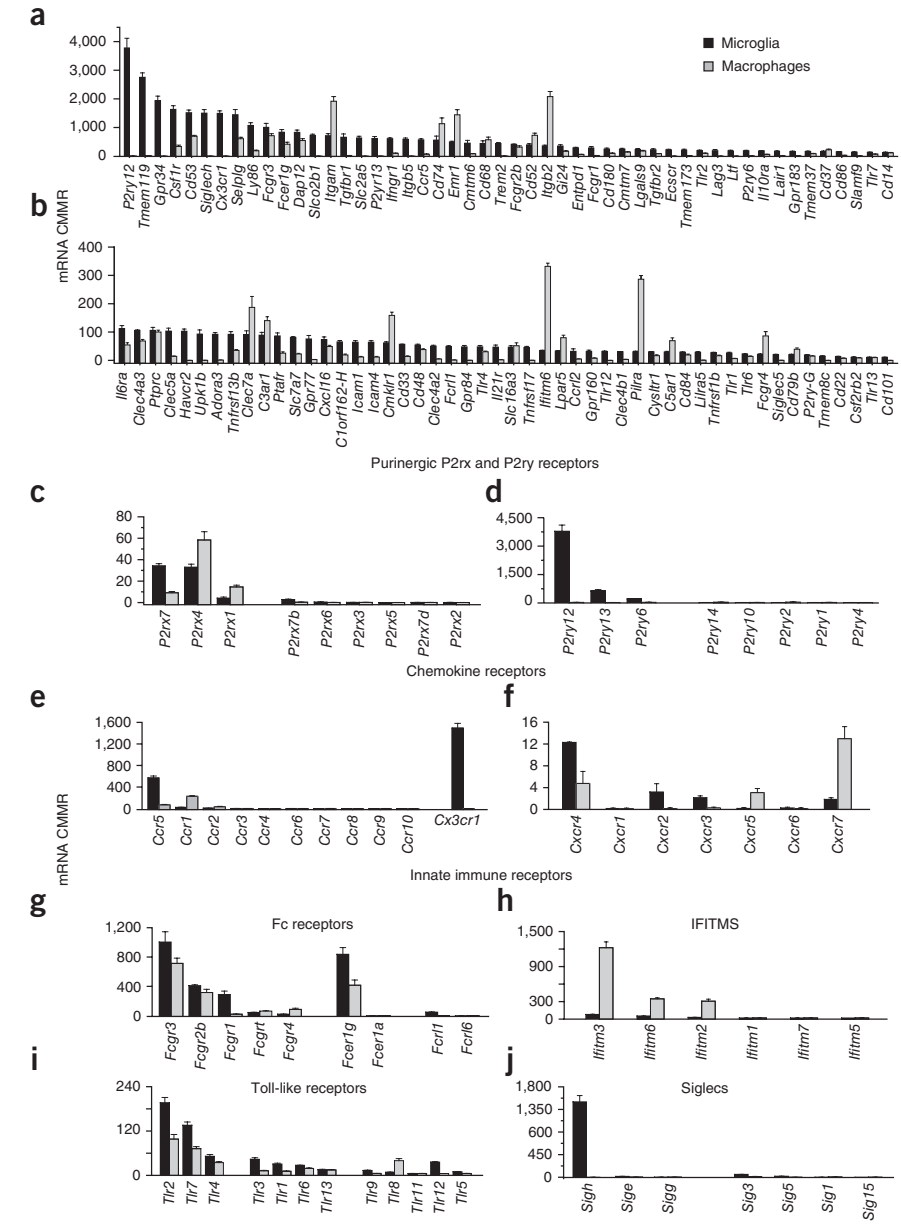

Figure 3 Comparative expression of the microglial and macrophages genes. Comparison of expression levels of sensome genes and those involved in regulating the immune response revealed a distinct immune signature for each cell type. (**a**,**b**) Expression levels of the microglial sensome in microglia and macrophages showed that several genes were differentially expressed. (**c**) Purinergic P2rx receptors. (**d**) Purinergic P2ry receptors. (**e**) Chemokine Ccr and Cx3cr1 receptors. (**f**) Chemokine Cxcr receptors. (**g**) Fc receptors. (**h**) Interferon-inducible transmembrane. (**i**) Toll-like receptors 1–13. (**j**) Sialic acid binding immunoglobulin lectins. Values are presented as mean ± s.d. of three different experiments carried out with microglia pooled from 22, 10 and 20 mice, and three pools of macrophages from ten mice per pool (see **Supplementary Table 2**).

transcripts that are not common to the other cell (**Fig. 2a**,**b**). Analysis of the 25 most highly expressed transcripts that were also uniquely expressed in microglia revealed expression levels ranging from 360–10,088 CMMR (**Fig. 2c**). These transcripts were highly enriched in microglia compared with macrophages ($P < 0.00001$, $\log_2$ fold change ranging from 4.8–15.1; **Supplementary Table 2**). These genes included several of the sensome genes discussed above, including *P2ry12*, *P2ry13*, *Tmem119*, *Gpr34*, *Siglech*, *Trem2* and *Cx3cr1* (**Fig. 2c** and **Supplementary Table 2**). In addition, microglia highly expressed several unique transcripts that we did not expect to be expressed only in these cells, including the enzyme hexosaminidase B (*Hexb*) and the antimicrobial peptides *Camp* and *Ngp* (**Fig. 2c** and **Supplementary Table 2**). The levels of expression of the top 25 transcripts unique to macrophages ranged from 596–15,327 CMMR ($P < 0.00001$ for all included transcripts; **Fig. 2d** and **Supplementary Table 2**) with a $\log_2$ fold change of 6.1–13.6, indicating a high level of enrichment regardless of the copy number of each transcript (**Supplementary Table 2**). Macrophage-enriched genes included fibronectin, the chemokine Cxcl13 and the endothelin B receptor (**Fig. 2d** and **Supplementary Table 2**).

To identify microglial sensome transcripts that are also expressed in macrophages, we compared expression of these genes in the two cell types. Sensome genes that were expressed in both microglia and macrophages include *Csfr1*, *Cd53*, *Selplg* and *Fcgr3*. Some microglial sensome genes were more highly expressed in macrophages, including *Itgam*, *Cd74*, *Emr1*, *Itgb2*, *Cd37*, *Clec7a*, *Cmklr1*, *Ifitm6*, *Pilra* and *Fcgr4*. Notably, of the 22 sensome genes that were exclusively expressed in microglia, 16 interacted with endogenous ligands rather than with pathogens (**Fig. 3a**,**b** and **Supplementary Table 2**). These data suggest that microglia express a unique set of genes, distinct from that of macrophages, that allow them to sense and interact with their local environment.

To further characterize the similarities and differences between macrophages and microglia, we compared the levels of expression of several specific gene families involved in immune responses, including purinergic receptors (P2y and P2x), chemokine receptors, Fc receptors, interferon-inducible transmembrane (Ifitms), Toll-like receptors (Tlrs), sialic acid–binding immunoglobulin lectins (Siglecs) and scavenger receptors (**Fig. 3c–j**, **Supplementary Fig. 2** and **Supplementary Table 2**). We found that microglia expressed significantly higher levels of several sensome genes, including *P2rx7*, *P2ry12*, *P2ry13*, *P2ry6*, *Ccr5*, *Cx3cr1*, *Cxcr4*, *Cxcr2*, *Tlr2*, *Siglech* and *Siglec3*, compared with macrophages (all $P < 0.00001$). In contrast, macrophages expressed significantly higher levels of *P2rx4*, *Ccr1*, *Cxcr7*, *Ifitm2*, *Ifitm3*, *Ifitm6* and *Tlr8* (all $P < 0.00001$). Notably, microglia expressed negligible levels of all Ifitm genes compared with macrophages.

Because DRS data is unbiased and quantitative, comparison of the transcriptomes of whole brain, microglia and macrophages allowed us to identify a distinct gene signature for microglia and provide a more concrete molecular definition of these cells. This signature includes a variety of genes with a wide range of functions (**Supplementary Fig. 3**). These genes not only reflect unique functional capabilities of

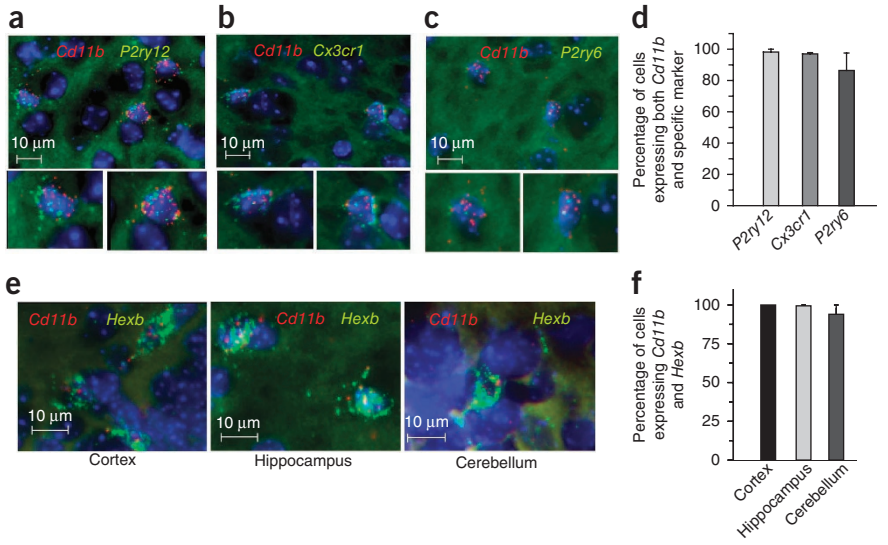

Figure 4 RNAscope dual fluorescence *in situ* hybridization. Dual RNAscope was performed on brain slices from adult mice for *Cd11b* and sensome genes with high (*P2ry12*), intermediate (*Cx3cr1*) and low (*P2ry6*) levels of expression and for the highly expressed *Hexb* gene. The results confirm DRS findings and revealed exclusive expression in microglia and no expression in *Cd11b*-negative cells. (**a**) Dual RNAscope for *Cd11b* (red) and *P2ry12* (green) probes, nuclei are stained with DAPI (blue). Bottom, magnified images of the double-positive cells shown at top. (**b**) Dual RNAscope for *Cd11b* (red) and *Cx3cr1* (green) probes. Bottom, magnified images of the double-positive cells shown at top. (**c**) Dual RNAscope for *Cd11b* (red) and *P2ry6* (green) probes. Bottom panels, magnified images of the double-positive cells shown at top. (**d**) Quantitative image analysis of RNAscope data for *Cd11b*$^+$ cells with *P2ry12* and *Cx3cr1* and *P2ry6*. (**e**) Dual RNAscope for *Cd11b* (red) and *Hexb* (green) probes in the cortex, hippocampus and cerebellum. (**f**) Nearly all of the *Cd11b*-positive cells in the cortex, hippocampus and cerebellum coexpressed *Hexb*. Data are presented as mean ± s.e.m.

microglia, but can also be used as microglial markers to identify these cells in physiologic conditions. Changes in expression levels of these genes under pathologic conditions could also be used as potential biomarkers for such conditions.

Validation of DRS by dual fluorescence *in situ* hybridization

To confirm that microglial sensome genes are only expressed in microglia and not in other brain cells, we performed dual RNAscope, a dual fluorescence *in situ* hybridization technique[37]. We used *Cd11b* as a universal microglial marker and three microglial sensome genes, *P2ry12*, *Cx3cr1* and *P2ry6*, with high, intermediate and low expression in microglia, respectively (**Fig. 1a**,**b** and **Supplementary Table 1**). *P2ry12*, *Cx3cr1* and *P2ry6* mRNA colocalized with *Cd11b* mRNA in the brain parenchyma of young mice (**Fig. 4a**–**c**). 98% of cells expressing *Cd11b* also expressed *P2ry12* and *Cx3cr1* and 87% also expressed *P2ry6* (**Fig. 4d**). Cells that did not express *Cd11b* mRNA did not hybridize with probes for *P2ry12*, *Cx3cr1* or *P2ry6*. These data support our DRS findings that microglial sensome genes are exclusively expressed in microglia in the brain.

An unexpected finding revealed by our DRS analysis is that *Hexb* was highly enriched in microglia compared with brain (**Supplementary Fig. 3a**). To determine whether *Hexb* is predominantly expressed in microglia *in situ*, we performed dual RNAscope on mouse brains using probes for *CD11b* and *Hexb*. As observed for *P2ry12*, *Cx3cr1*

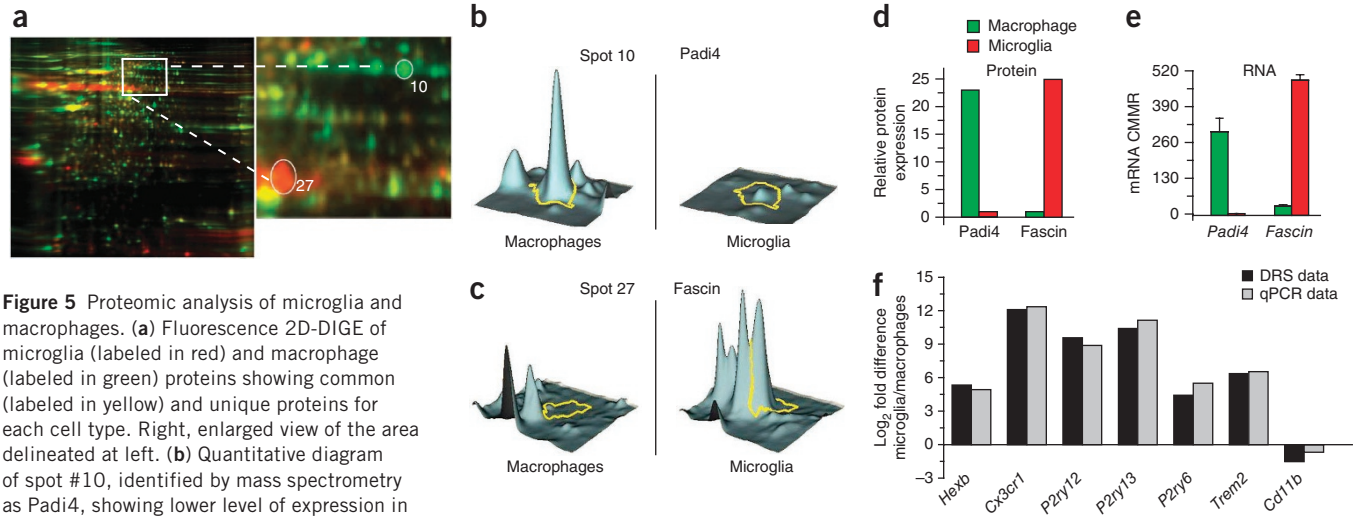

Figure 5 Proteomic analysis of microglia and macrophages. (**a**) Fluorescence 2D-DIGE of microglia (labeled in red) and macrophage (labeled in green) proteins showing common (labeled in yellow) and unique proteins for each cell type. Right, enlarged view of the area delineated at left. (**b**) Quantitative diagram of spot #10, identified by mass spectrometry as Padi4, showing lower level of expression in microglia compared with macrophage. (**c**) Quantitative diagram of spot #27, identified by mass spectrometry as fascin, showing higher level of expression in microglia compared with macrophage. (**d**,**e**) Comparison of protein levels (measured by mass spectrometry) and mRNA levels (measured by DRS) of Padi4 and fascin in macrophage and microglia. DRS values are presented as mean ± s.d. of three different experiments carried out with microglia pooled from 22, 10 and 20 mice, and from three pools of macrophages from ten mice per pool. Protein values are from pooled microglia and macrophages isolated from 70 and 50 mice, respectively. (**f**) Validation by qPCR of some genes obtained with DRS on new cohorts of mice. The new cohorts comprised five sorted microglia pools and six macrophage pools from sorting of six sets using five mice per set. Ratio values for qPCR and DRS data represent the ratio of the gene of interest to B2-micoglobulin expression. Data are plotted as $\log_2$ fold difference between microglia/macrophage ratio values.

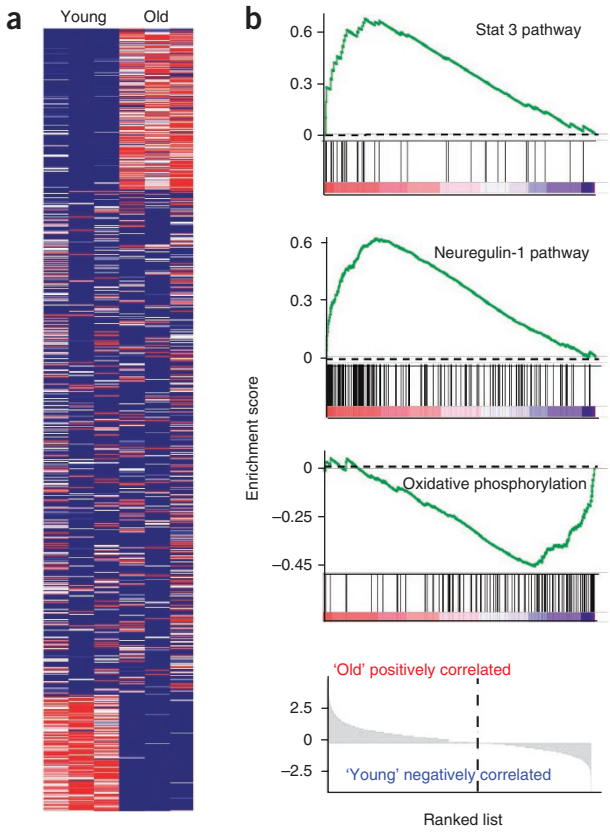

Figure 6 Effects of aging on the microglial mRNA expression profile. (**a**) Heat map of the 10,598 microglial transcripts expressed at >1 CMMR revealed that 1,831 transcripts were upregulated, 1,672 were downregulated and 7,095 remained unchanged with aging. (**b**) GSEA pathways analysis showed upregulation of potentially neuroprotective pathways, including Stat 3 and Neuregulin-1, and downregulation of potentially neurotoxic pathways, including oxidative phosphorylation. Each bar at the bottom of each panel represents a member gene of the respective pathway and shows its relative location in the ranked list of genes (lowest panel).

and *P2ry6*, *Hexb* mRNA also colocalized with *CD11b* in the cortex, hippocampus and cerebellum (**Fig. 4e**). Nearly all cells expressing *CD11b* also expressed *Hexb* (**Fig. 4e**,**f**). Cells that did not express *CD11b* mRNA did not hybridize with probes for *Hexb* (**Fig. 4e** and data not shown). These data support our finding that *Hexb* mRNA is exclusively expressed in microglia in the brain.

Proteomic and qPCR analysis of microglia and macrophages

To determine whether levels of mRNA transcripts compare with protein expression, we evaluated protein expression differences between microglia and macrophages by two-dimensional difference gel electrophoresis (2D-DIGE) and compared the results with DRS data for the proteins identified. Protein samples were extracted from each cell type and labeled with CyDye (microglia in red and macrophages in green), mixed and loaded onto the same two-dimensional electrophoresis gel. Red protein spots represented microglia-enriched proteins, green spots represented macrophage-enriched proteins and yellow spots represented proteins expressed in both cell types (**Fig. 5a**). To insure unbiased analysis, we randomly selected 30 spots of interest (15 green and 15 red) excised them from the gel and determined protein identity via mass spectrometry (*Padi4* and *Fascin* are presented as examples; **Fig. 5a**–**c**). The mRNA level for each of these proteins (CMMR) was obtained from our DRS data set. Protein and mRNA levels of both *Padi4* and *Fascin* exhibited similar trends in expression (**Fig. 5d**,**e**). Of the 30 proteins identified, 22 exhibited similar trends of expression between protein and mRNA levels (**Supplementary Fig. 4** and data not shown). In the remaining eight proteins identified, substantial differences were observed in the mRNA levels between microglia and macrophages, but not in the protein levels (data not shown). An advantage of this approach is that it allows unbiased comparison between protein and mRNA levels, as protein identification is made after the spots are selected. A limitation of this approach is that it only allows assessment of proteins that are intracellular or membrane proteins that are resistant to the proteases collagenase and dispase, the two enzymes that we used to purify microglia. Nonetheless, our data show that expression levels of a majority of the proteins identified correlate with their respective mRNA levels, thereby providing added validation for our DRS analysis.

We further validated our DRS data by qPCR using a new cohort of mice. Microglia and macrophages from 30 5-month-old mice were isolated as described above for DRS and divided into five and six pools, respectively. We then performed qPCR analysis on seven transcripts, including *Hexb*, *Cx3cr1*, *P2ry12*, *P2ry13*, *P2ry6*, *Trem2* and *Cd11b*. As seen in our DRS analysis, *Hexb*, *Cx3cr1*, *P2ry12*, *P2ry13*, *P2ry6* and *Trem2* were highly expressed on microglia compared with macrophages (**Figs. 2a** and **3a**,**b**). In contrast, CD11b is more highly expressed on macrophages than microglia (**Supplementary Fig. 1**). We compared qPCR and DRS data by quantifying the $\log_2$ of the ratio of microglia and macrophages. The results obtained from qPCR and DRS were highly comparable, indicating that our DRS data is strongly supported by qPCR data on a different set of mice (**Fig. 5f**). These results further confirm the validity of our DRS data.

Effects of aging on the microglial biological pathways

Aging is associated with substantial alteration of the gene expression profile of the whole brain[38]. To determine the effects of aging on the microglia transcriptome, we used DRS to identify the transcriptome of microglia isolated from 24-month-old mice and compared it with that of microglia isolated from 5-month-old mice as described above. We limited the analysis to transcripts expressed at ≥1 CMMR. Of these 10,598 transcripts, 3,503 transcripts were significantly different between young and old microglia ($P < 0.05$), 1,831 were upregulated, 1,672 were downregulated and the remainder were not significantly changed in old versus young microglia ($P > 0.05$; **Fig. 6a**).

We performed GSEA (Online Methods) to identify pathways that are differentially changed in aging microglia. An interesting trend emerged from our analysis. Several pathways that have been described previously as promoting neurotoxicity appeared to be downregulated in older microglia. In contrast, pathways involved in neuroprotection appeared to be upregulated (**Fig. 6b** and **Supplementary Figs. 5** and **6**). Genes involved in Stat3 (ref. 39) and Neuregulin-1 (ref. 40) pathways are upregulated in older mice, whereas those associated with oxidative phosphorylation[41] pathways are down-regulated.

Effects of aging on the microglial priming state

Microglia exhibit various priming states that determine their responses to subsequent injury or infection of the brain. Interferon-γ induces microglia to assume the classical priming state, which is associated with a neurotoxic phenotype promoting neuronal degeneration. In contrast, the alternative priming state, associated with exposure of these cells to IL4 or IL13, is neuroprotective and promotes axonal

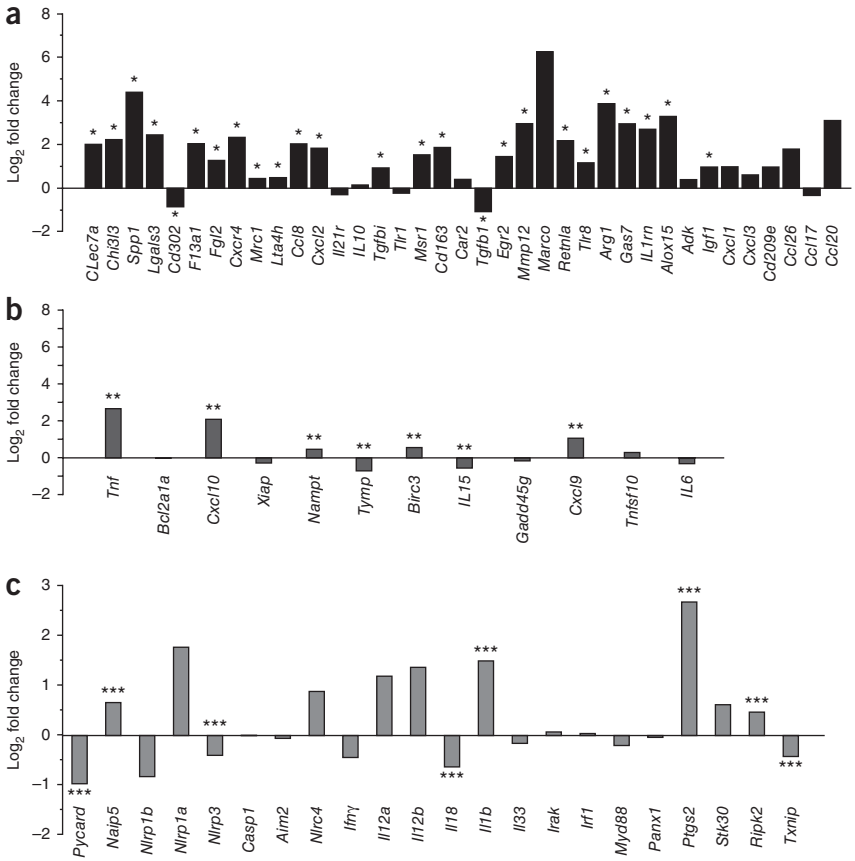

Figure 7 Upregulation of alternative priming genes in microglia from aged mice. (**a**,**b**) Alternative and classical priming genes in microglia from 24-month-old mice compared with 5-month-old mice revealed a wide range of expression levels. In old mice (**a**), 24 of 37 alternative priming state markers were significantly upregulated (*$P < 0.016$). In microglia from 24-month-old mice (**b**), 5 of 12 markers of the classical priming state were significantly upregulated in microglia compared with 5-month-old mice (**$P < 0.017$), whereas the remaining 7 were downregulated or not significantly changed. (**c**) Analysis of 22 inflammasome-associated genes revealed that 4 were significantly upregulated in old mice compared with young ones (***$P < 0.025$), whereas the remaining 18 genes were downregulated or not significantly changed. Taken together, the data suggest a trend toward increased expression of genes involved in resolution of inflammation and neuroprotection. Values are presented as $\log_2$ fold change of three different experiments carried out with microglia pooled from 22, 10 and 20 young mice, and from three pools of ten mice from old mice (see **Supplementary Table 3**).

sprouting and elongation[8,12]. Each priming state is characterized by increased expression of a defined set of genes that regulate microglial behavior and are considered markers for the corresponding priming state[11].

To determine the effect of aging on the microglial priming state, we compared expression of classical and alternative priming genes[10,42] in microglia isolated from 5-month-old and 24-month-old mice. We found that, in microglia from 24-month-old mice, expression of alternative priming markers ranged between 6–348 CMMR and classical priming markers were expressed between 4 and 105 CMMR (**Supplementary Table 3**). 62% (23 of 37) of alternative priming markers were significantly upregulated in microglia from aged mice (mean $\log_2$ fold change = 1.97, $P < 0.012$), whereas 32% (12 of 37) were not significantly changed ($P > 0.05$) and only CD302 and TGFβ1 were downregulated (**Fig. 7a** and **Supplementary Table 3**). In contrast, aging was associated with downregulation or no change in 7 of 12 (58%) of the classical priming state markers (mean fold enrichment over brain ($\log_2$ fold change) = 0.37; **Fig. 7b** and **Supplementary Table 3**). These data suggest that a shift occurs during aging in the microglial phenotype toward an alternative neuroprotective priming state.

We also analyzed changes in expression of 22 inflammasome-associated genes. Notably, 82% (18 of 22) of the inflammasome genes included in our analysis were either significantly downregulated ($P < 0.025$) or not significantly changed ($P > 0.05$; **Fig. 7c** and **Supplementary Table 3**). Given that upregulation of some inflammasome genes, including *Nlrp3*, have been implicated in the pathogenesis of Alzheimer's disease[43], these findings further support the idea that there is a shift of the microglial phenotype toward an alternative neuroprotective priming state during normal aging.

Effects of aging on the microglial sensome

We also assessed any age-related changes in the microglial sensome genes and in selected families of genes. We found that 31% (31 of 100) of the sensome genes were significantly downregulated with aging ($P < 0.043$) and 13% were significantly upregulated with aging ($P < 0.008$) (**Fig. 8a** and **Supplementary Table 3**). Notably, 81% of the genes that were significantly downregulated (25 of 31 genes) encoded proteins involved in sensing endogenous ligands, whereas 62% (8 of 13) of the genes that were upregulated encoded proteins involved in sensing infectious microbial ligands (**Fig. 8a** and **Supplementary Tables 1** and **3**). Genes that were significantly downregulated encoded proteins involved in sensing apoptotic neurons (Trem2, $P < 0.00005$), substances released following neuronal injury, such as nucleotides and adenosine, and molecules expressed in the cell surface (siglech, $P = 0.003$; Dap12, $P = 0.00005$) and soluble cytokines (*Ccr5*, $P = 0.0006$; *Ifngr1*, $P = 0.00033$). Genes that were significantly upregulated encoded proteins involved in sensing bacterial and fungal ligands (Tlr2, CD74, Ltf, Clec7a, Cxcl16 and Ifitm6, all $P \leq 0.0006$) or bacterial toxins (C5ar1, $P < 0.00005$) (**Fig. 8** and **Supplementary Tables 1** and **3**).

Among the chemokine receptors, expression of *Cxcr4* and *Cxcr2* was significantly ($P \leq 0.0001$) increased in aged microglia (**Fig. 8e** and **Supplementary Table 3**). Of note, there were significant changes in the expression of members of the Ifitm family of innate immune receptors. Significant increases were seen in Ifitm2, Ifitm3 and Ifitm6 (all $P \leq 0.0001$; **Fig. 8g**, and **Supplementary Table 3**).

DISCUSSION

Our data fill several major gaps in our understanding of microglia. First, the use of direct RNA sequencing allowed us to generate a quantitative data set of the normal adult microglia transcriptome, representing an accurate snapshot of these cells' gene expression profile. This is the only such data set available at this point for any cell type

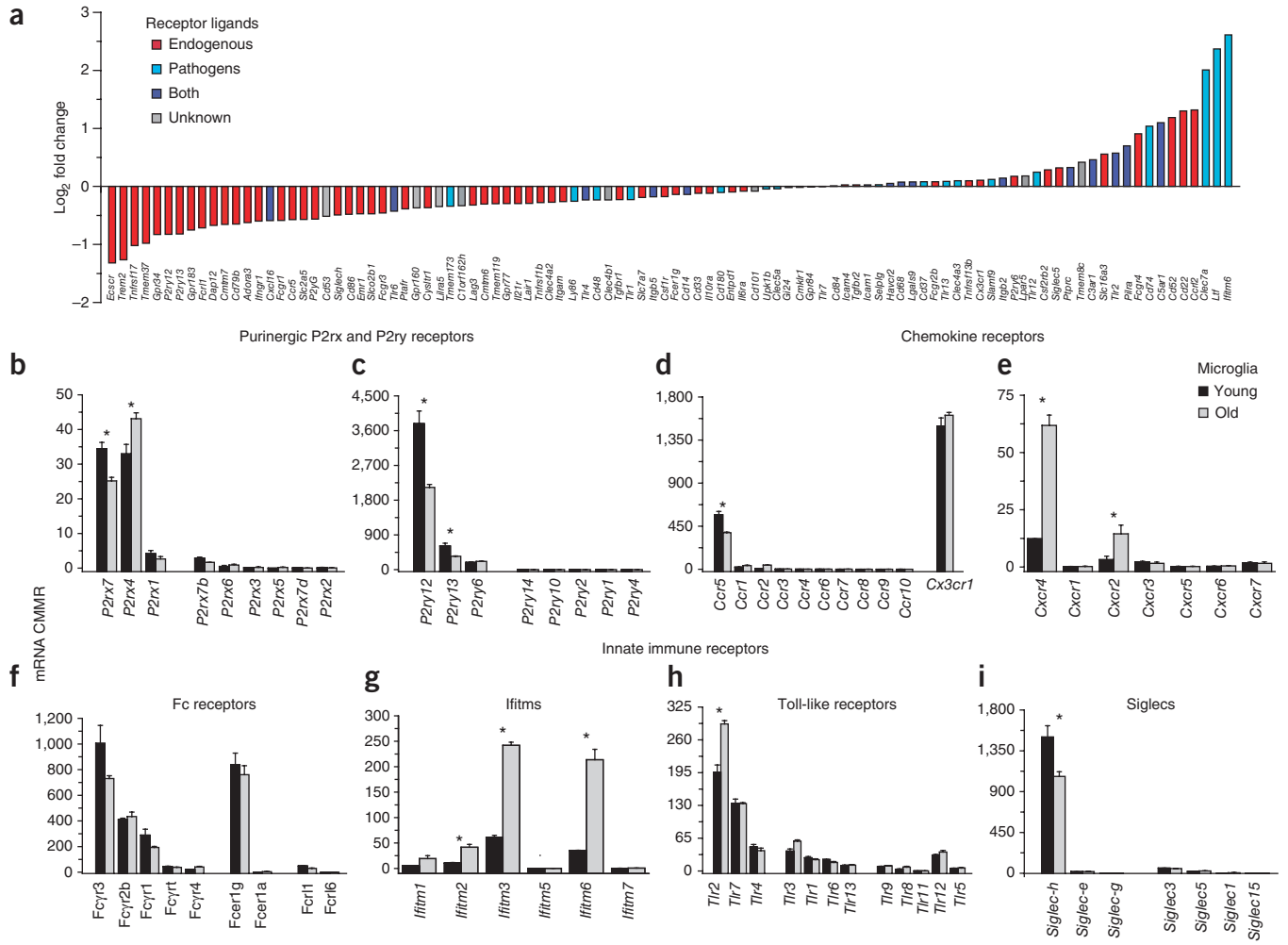

Figure 8 The microglial sensome in aging. (**a**) Measurement of the $\log_2$ fold change of genes encoding the microglial sensome, as determined by DRS, revealed that ~81% of the genes were significantly downregulated (*Escr1→Tmem173*, $P < 0.043$) and encode proteins that are involved in sensing endogenous ligands (red bars). Of the 69 genes that were unchanged or upregulated, 45% encode proteins that are involved in sensing infectious microbial ligands (blue bars and purple bars). Of the genes that were significantly upregulated, ~62% (*C3ar1→Ifitm6*, $P < 0.008$) encode proteins that are involved in pathogen sensing and host defense. (**b**–**i**) Comparative expression of genes involved in regulating the immune response in old versus young microglia revealed a selective set of genes that were changed with normal aging. Values are presented as mean ± s.d. of three different experiments carried out with microglia pooled from 22, 10 and 20 young mice, and from three pools of microglia from ten mice per pool. $*P < 0.03$.

of the mammalian brain. Our data set avoids the potential pitfalls associated with other approaches to studying gene expression because it does not involve cDNA synthesis or amplification. Our data also differ from semiquantitative data sets in that we provide copy numbers of each transcript rather than relative arbitrary units, making it possible to compare our data with similar data sets generated in the future. The ability to perform such a comprehensive study using small amounts of unamplified RNA provides a proof of concept that this approach can be applied to various cells from different healthy and diseased mammalian tissues. One can envision using DRS on cells obtained from biopsy samples, providing a more personalized approach to understand gene expression profiling in the brain. The strength of our data is highlighted by the correlation between the copy number of each transcript obtained by DRS with *in situ* hybridization and the relative protein expression of several proteins as determined by unbiased proteomic analysis using 2D-DIGE and mass spectrometry of 30 proteins and by qPCR of several genes.

Second, we introduce a new area of investigation, namely that of the microglial sensome. We identified 100 genes that constitute the microglial toolset for sensing changes in the brain's milieu. Given that sensing of the brain environment is a major function of microglia, our data define the apparatus that microglia use to perform these homeostatic functions, including sensing of chemokines and cytokines, purinergic molecules, inorganic substances, changes in pH, and amino acids. Defining the microglial sensome under physiological conditions establishes a baseline to which we can compare and identify changes that occur in this sensome under pathological conditions. As an example, we performed studies to identify changes in the sensome that occur with aging and found substantial changes. Defining changes in the sensome that accompany infection, neurodegeneration, traumatic brain injury and inherited disorders is likely to have substantial implications for identifying biomarkers, as well as new therapeutic modalities for such disorders[44]. Highlighting the importance of our data set, two members of the microglial sensome, *Trem2* and *Cd33*, are independent risk factors for late-onset Alzheimer's disease[30–32]. We propose that several additional members of the microglial sensome are also important in a number of CNS disorders.

Third, we compared the copy number of each transcript in microglia, whole brain and macrophages and were able to identify a molecular signature that defines microglia and distinguishes these cells from other types of resident macrophages and other cells in the brain. Such analyses yielded some expected results, including the high level of expression of the purinergic receptor *P2ry12*, the chemokine receptor *Cx3cr1* and *Trem2*, the receptor for apoptotic neurons in microglia. In addition, our data included some unexpected findings. For example, we found that the enzyme hexosaminidase B (*Hexb*) was predominantly a microglial enzyme in the brain. The level of expression of this transcript in microglia indicates it is one of the most highly expressed mRNAs in these cells. *Hexb* mRNA was enriched 164-fold in microglia compared with brain, more than the level of enrichment of the quintessential microglial marker *Cx3cr1* (142.5-fold enrichment) and *CD11b* (98.8-fold enrichment), one of the two markers that we used to identify microglia. These data indicate that *Hexb* is indeed a microglial gene. We further confirmed this observation using dual RNAscope fluorescence *in situ* hybridization. Given that *Hexb* mutations result in the neurodegenerative gangliosidosis Sandhoff disease[45], this finding has substantial implications for our understanding of this disease, suggesting that this inherited disorder is essentially a 'microglia' disorder. This suggests that microglia, rather than neurons, may be better targets for therapeutic intervention in this disorder. This is an example of the usefulness of our data and their potential for altering our understanding of microglial biology in sickness and in health. Another likely implication from these findings is the identification of several new microglial markers. In this regard, our data complements and adds to recent microarray data[46]. Indeed, 32% of transcripts of the microglial sensome have not been described in microglia.

We also found that resting microglia expressed high levels of several antimicrobial peptides that have not previously been observed in these cells, including *Camp* (cathelin-related antimicrobial peptide, 633 CMMR) and *Ngp* (neutrophilic granule protein, 424 CMMR). The high level of expression of these peptides indicates a high level of readiness by the normal, 'quiescent' resident microglia to perform its innate host defense function in the absence of adaptive immune molecules and cells.

Fourth, we identified several age-related changes in the microglial transcriptome. For example, the microglial sensome is substantially altered during aging. More than 81% of the sensome genes that were downregulated during aging are involved in sensing endogenous ligands. Of particular interest are purinergic and associated receptors, such as *P2yr12*, *P2ry13* and *Adora3*, and receptors recognizing apoptotic neurons and other cells, such as *Siglech*. Purinergic molecules are released with neuronal injury and cell death, events that are likely to increase with aging. The continuous stimulation of microglia that could result from the excessive neuronal injury and death that accompany aging may initiate a cycle of events that leads to further microglial-mediated neurotoxicity, adding insult to injury. It is therefore conceptually beneficial to the brain to downregulate the ability of microglia to get activated by dying or injured cells with aging. Notably, sensing genes involved in phagocytosis, such as *Cd11b*, *Cd14*, *Cd68* and ICAM genes, are unchanged, suggesting that the ability to clear endogenous debris is not affected. Similarly, genes that mediate the ability of microglia to sense microbial ligands are neither affected nor increased. These data contrast with what happens in advanced stages of neurodegenerative disorders such as Alzheimer's disease, multiple sclerosis and amyotrophic lateral sclerosis, where microglia become neurotoxic[7–9]. These data also contrast with recent findings of neurotoxic aging associated changes in the peripheral immune system[47]. Our data suggest that there is a shift with aging in the microglial phenotype toward a more neuroprotective type. Although the peripheral immune system may become more primed toward a neurotoxic state[47], our data suggest that the microglia retain their ability to defend against infectious pathogens and clear debris, but attempt to 'tone down' the stimulatory effects of endogenous debris, as if to keep from becoming constantly activated.

Taken at face value, our data appear to conflict with reports that suggest that aging is accompanied by an overall increase in the pro-inflammatory status of the brain[48–50]. An important distinction between these studies and ours is that the previous studies were done using whole brain tissue rather than purified cells. Changes observed in these studies reflect not only the gene expression profiles of microglia, but also those of other glial cells and possibly circulating blood leukocytes. Furthermore, these studies either included a limited number of genes[48] or involved injecting the brain with a cocktail of cytokines before gene expression analysis[50]. These technical differences may explain the differences in our results and these other studies.

Supporting the idea that there is an aging-associated change in the microglial phenotype toward a more neuroprotective state, we found that several potential neurotoxic pathways, including the oxidative phosphorylation pathway, were downregulated in microglia with aging[41]. In contrast, pathways that may be neuroprotective, such as the Stat3 and Neuregulin-1 pathways, were upregulated. Furthermore, the microglial priming state was also altered in aging toward an alternative phenotype. Classical and alternative priming states are not activation states, but rather priming states that dictate how the microglia will respond to a certain stimulus. In spinal cord injury, for example, an alternative priming state is associated with improved axonal sprouting and elongation, indicating a neuroprotective phenotype[12]. Genes that are upregulated in an alternative primed state, such as *MRC1*, *Dectin* and *Lgals3*, favor phagocytosis of debris and pathogens. Other genes, such as *Arg1* and *IL1rn*, downregulate the innate response possibly reducing the damage associated with such a response. Arg1 induces a shift in arginine metabolism from interferon-γ–induced nitric oxide production toward production of ornithine and polyamine, which are important in wound healing. Similarly, IL1rn antagonizes the effects of IL1 (ref. 10). Taken together, our data suggest that aging is associated with a shift in the microglial gene expression profile toward a more neuroprotective phenotype. We propose that when the brain is faced with an injury or stimulus that acutely activates the microglia, the alternative primed state assumed by these cells with aging may not completely prevent the damages induced by the injurious stimuli, but will likely help to reduce the effects of such damage.

Our approach and data represent a major step toward establishing a definitive quantitative microglia transcriptome under a variety of pathological situations. Understanding the changes that occur in the microglia in aging, neurodegeneration, infection and traumatic injury is the first step in identifying therapeutics that modulate the state of these cells and, ultimately, alter disease processes.

METHODS

Methods and any associated references are available in the online version of the paper.

Accession codes. The Direct RNA sequencing data has been deposited in the NCBI BioProject database under the BioProject ID code PRJNA219501.

Note: Any Supplementary Information and Source Data files are available in the online version of the paper.

ACKNOWLEDGMENTS

We thank F. Ozsolak (Helicos) for supervising the sequencing experiments, R. Mylvaganam for performing cell sorting and J. Liao (Applied Biomics) for analysis of the proteomic data. This work was supported by grants from the National Institute of Neurological Disorders and Stroke (NS059005) and the National Institute of Aging (AG032349) to J.E.K.

AUTHOR CONTRIBUTIONS

S.E.H. co-designed the experiments performed all cell isolations from peritoneum and brain, RNA extractions and quality analysis and co-wrote the manuscript. N.D.K. assisted in all cell isolations and sorting for DRS and proteomics studies. T.K.O. and M.L.B. performed bioinformatics analyses, including development of programs in MolBioLib to annotate sequence information obtained from Helicos. L.W. performed the RNAscope experiments. T.K.M. was involved in designing experiments and data analysis. J.E.K. co-designed the experiments, analyzed the data and co-wrote the manuscript.

COMPETING FINANCIAL INTERESTS

The authors declare no competing financial interests.

1. Lawson, L.J., Perry, V.H., Dri, P. & Gordon, S. Heterogeneity in the distribution and morphology of microglia in the normal adult mouse brain. *Neuroscience* **39**, 151–170 (1990).
2. El Khoury, J. *et al.* Ccr2 deficiency impairs microglial accumulation and accelerates progression of Alzheimer-like disease. *Nat. Med.* **13**, 432–438 (2007).
3. Rezaie, P. & Male, D. Mesoglia & microglia–a historical review of the concept of mononuclear phagocytes within the central nervous system. *J. Hist. Neurosci.* **11**, 325–374 (2002).
4. Nimmerjahn, A., Kirchhoff, F. & Helmchen, F. Resting microglial cells are highly dynamic surveillants of brain parenchyma *in vivo*. *Science* **308**, 1314–1318 (2005).
5. Block, M.L., Zecca, L. & Hong, J.S. Microglia-mediated neurotoxicity: uncovering the molecular mechanisms. *Nat. Rev. Neurosci.* **8**, 57–69 (2007).
6. Gomes-Leal, W. Microglial physiopathology: how to explain the dual role of microglia after acute neural disorders? *Brain Behav.* **2**, 345–356.
7. Hickman, S.E., Allison, E.K. & El Khoury, J. Microglial dysfunction and defective beta-amyloid clearance pathways in aging Alzheimer's disease mice. *J. Neurosci.* **28**, 8354–8360 (2008).
8. Liao, B., Zhao, W., Beers, D.R., Henkel, J.S. & Appel, S.H. Transformation from a neuroprotective to a neurotoxic microglial phenotype in a mouse model of ALS. *Exp. Neurol.* **237**, 147–152 (2012).
9. Muzio, L., Martino, G. & Furlan, R. Multifaceted aspects of inflammation in multiple sclerosis: the role of microglia. *J. Neuroimmunol.* **191**, 39–44 (2007).
10. Gordon, S. & Martinez, F.O. Alternative activation of macrophages: mechanism and functions. *Immunity* **32**, 593–604 (2010).
11. Colton, C.A. Heterogeneity of microglial activation in the innate immune response in the brain. *J. Neuroimmune Pharmacol.* **4**, 399–418 (2009).
12. Kigerl, K.A. *et al.* Identification of two distinct macrophage subsets with divergent effects causing either neurotoxicity or regeneration in the injured mouse spinal cord. *J. Neurosci.* **29**, 13435–13444 (2009).
13. Kang, H.J. *et al.* Spatio-temporal transcriptome of the human brain. *Nature* **478**, 483–489 (2011).
14. Berchtold, N.C. *et al.* Gene expression changes in the course of normal brain aging are sexually dimorphic. *Proc. Natl. Acad. Sci. USA* **105**, 15605–15610 (2008).
15. Kremsky, I., Morgan, T.E., Hou, X., Li, L. & Finch, C.E. Age-changes in gene expression in primary mixed glia cultures from young vs. old rat cerebral cortex are modified by interactions with neurons. *Brain Behav. Immun.* **26**, 797–802 (2012).
16. VanGuilder, H.D., Vrana, K.E. & Freeman, W.M. Twenty-five years of quantitative PCR for gene expression analysis. *Biotechniques* **44**, 619–626 (2008).
17. Schena, M. *et al.* Microarrays: biotechnology's discovery platform for functional genomics. *Trends Biotechnol.* **16**, 301–306 (1998).
18. Schena, M., Shalon, D., Davis, R.W. & Brown, P.O. Quantitative monitoring of gene expression patterns with a complementary DNA microarray. *Science* **270**, 467–470 (1995).
19. Geiss, G.K. *et al.* Direct multiplexed measurement of gene expression with color-coded probe pairs. *Nat. Biotechnol.* **26**, 317–325 (2008).
20. Nagalakshmi, U. *et al.* The transcriptional landscape of the yeast genome defined by RNA sequencing. *Science* **320**, 1344–1349 (2008).
21. Nagalakshmi, U., Waern, K. & Snyder, M. RNA-Seq: a method for comprehensive transcriptome analysis. *Curr. Protoc. Mol. Biol.* **4.11**, 1–13 (2010).
22. Ozsolak, F. *et al.* Direct RNA sequencing. *Nature* **461**, 814–818 (2009).
23. El Khoury, J.B. *et al.* CD36 mediates the innate host response to beta-amyloid. *J. Exp. Med.* **197**, 1657–1666 (2003).
24. Sedgwick, J.D. *et al.* Isolation and direct characterization of resident microglial cells from the normal and inflamed central nervous system. *Proc. Natl. Acad. Sci. USA* **88**, 7438–7442 (1991).
25. Ohsumi, T.K. & Borowsky, M.L. MolBioLib: A C.11 framework for rapid development and deployment of bioinformatics tasks. *Bioinformatics* **28**, 2412–2416 (2012).
26. Subramanian, A. *et al.* Gene set enrichment analysis: a knowledge-based approach for interpreting genome-wide expression profiles. *Proc. Natl. Acad. Sci. USA* **102**, 15545–15550 (2005).
27. Robinson, M.D., McCarthy, D.J. & Smyth, G.K. edgeR: a Bioconductor package for differential expression analysis of digital gene expression data. *Bioinformatics* **26**, 139–140 (2010).
28. El Khoury, J. *et al.* Scavenger receptor-mediated adhesion of microglia to beta-amyloid fibrils. *Nature* **382**, 716–719 (1996).
29. Huang, D.W., Sherman, B.T. & Lempicki, R.A. Systematic and integrative analysis of large gene lists using DAVID bioinformatics resources. *Nat. Protoc.* **4**, 44–57 (2009).
30. Guerreiro, R. *et al.* TREM2 variants in Alzheimer's disease. *N. Engl. J. Med.* **368**, 117–127 (2013).
31. Jonsson, T. *et al.* Variant of TREM2 associated with the risk of Alzheimer's disease. *N. Engl. J. Med.* **368**, 107–116 (2013).
32. Bradshaw, E.M. *et al.* CD33 Alzheimer's disease locus: altered monocyte function and amyloid biology. *Nat. Neurosci.* **16**, 848–850 (2013).
33. Griciuc, A. *et al.* Alzheimer's disease risk gene CD33 inhibits microglial uptake of amyloid beta. *Neuron* **78**, 631–643 (2013).
34. von Mering, C. *et al.* STRING: a database of predicted functional associations between proteins. *Nucleic Acids Res.* **31**, 258–261 (2003).
35. Thrash, J.C., Torbett, B.E. & Carson, M.J. Developmental regulation of TREM2 and DAP12 expression in the murine CNS: implications for Nasu-Hakola disease. *Neurochem. Res.* **34**, 38–45 (2009).
36. Kettenmann, H., Hanisch, U.K., Noda, M. & Verkhratsky, A. Physiology of microglia. *Physiol. Rev.* **91**, 461–553 (2011).
37. Wang, F. *et al.* RNAscope: a novel in situ RNA analysis platform for formalin-fixed, paraffin-embedded tissues. *J. Mol. Diagn.* **14**, 22–29 (2012).
38. Colantuoni, C. *et al.* Temporal dynamics and genetic control of transcription in the human prefrontal cortex. *Nature* **478**, 519–523 (2011).
39. Dziennis, S. & Alkayed, N.J. Role of signal transducer and activator of transcription 3 in neuronal survival and regeneration. *Rev. Neurosci.* **19**, 341–361 (2008).
40. Xu, Z. *et al.* Neuroprotection by neuregulin-1 following focal stroke is associated with the attenuation of ischemia-induced pro-inflammatory and stress gene expression. *Neurobiol. Dis.* **19**, 461–470 (2005).
41. Reynolds, A., Laurie, C., Mosley, R.L. & Gendelman, H.E. Oxidative stress and the pathogenesis of neurodegenerative disorders. *Int. Rev. Neurobiol.* **82**, 297–325 (2007).
42. Martinez, F.O., Helming, L. & Gordon, S. Alternative activation of macrophages: an immunologic functional perspective. *Annu. Rev. Immunol.* **27**, 451–483 (2009).
43. Heneka, M.T. *et al.* NLRP3 is activated in Alzheimer's disease and contributes to pathology in APP/PS1 mice. *Nature* **493**, 674–678 (2013).
44. El Khoury, J. Neurodegeneration and the neuroimmune system. *Nat. Med.* **16**, 1369–1370 (2010).
45. Sango, K. *et al.* Mouse models of Tay-Sachs and Sandhoff diseases differ in neurologic phenotype and ganglioside metabolism. *Nat. Genet.* **11**, 170–176 (1995).
46. Gautier, E.L. *et al.* Gene-expression profiles and transcriptional regulatory pathways that underlie the identity and diversity of mouse tissue macrophages. *Nat. Immunol.* **13**, 1118–1128 (2012).
47. Villeda, S.A. *et al.* The ageing systemic milieu negatively regulates neurogenesis and cognitive function. *Nature* **477**, 90–94 (2011).
48. Cribbs, D.H. *et al.* Extensive innate immune gene activation accompanies brain aging, increasing vulnerability to cognitive decline and neurodegeneration: a microarray study. *J. Neuroinflammation* **9**, 179 (2012).
49. Lee, C.K., Weindruch, R. & Prolla, T.A. Gene-expression profile of the ageing brain in mice. *Nat. Genet.* **25**, 294–297 (2000).
50. Lee, D.C. *et al.* Aging enhances classical activation but mitigates alternative activation in the central nervous system. *Neurobiol. Aging* **34**, 1610–1620 (2013).

ONLINE METHODS

Mice. 5-month-old and 24-month-old C57BL/6 mice were purchased from the National Institute on Aging and housed in the animal care facility at Massachusetts General Hospital and used within 2 weeks of arrival. Mice were killed according to approved institutional procedures. All protocols were approved by the Massachusetts General Hospital Institutional Animal Care and Use Committee and met US National Institutes of Health guidelines for the humane care of animals.

Peritoneal macrophages. Peritoneal cells were harvested from 5-month-old mice by peritoneal lavage with 10 ml phosphate-buffered saline without Ca^{2+} and Mg^{2+} (PBS) containing 1 mM EDTA (PBS/EDTA) and centrifuged at 400*g* for 10 min. The peritoneal cells were then stained for CD11b and CD45 for flow cytometry (see below). Each sorting experiment was performed on cells pooled from five mice per experiment.

Microglia. Two ages of mice were used for isolation of microglia: 5 and 24 months old. Mice were perfused with 50 ml PBS. Brains were then removed, rinsed in PBS and placed separately into a GentleMacs C-tube (Miltenyi Biotech) with RPMI (no phenol red) containing 2 mM L-glutamine (Mediatech), Dispase (2 U ml^{-1}) and 0.2% Collagenase Type 3 (Worthington Biochemicals) according to our previous protocol[7]. Brains were processed using the gentleMACS Dissociator (Miltenyi Biotech) on the brain program settings according to manufacturer's directions. Briefly, the brains were subjected to three rounds of dissociation, each followed by a period of incubation at 37 °C. After the second round of dissociation, DNase I grade II (Roche Applied Science) was added to a concentration of 40 U ml^{-1} and incubated for an additional 10 min before the final round of dissociation. The digestion enzymes were inactivated by addition of PBS/EDTA containing 5% fetal bovine serum (FBS) and the digested brain bits were triturated gently, passed over a 100-µm filter (Fisher Scientific) and centrifuged. Cell pellets were resuspended in 10.5 ml RPMI 1640 (Gibco 1183530), mixed gently with 4.5 ml physiologic Percoll (Sigma Aldrich), and centrifuged at 850*g* for 40 min. The resulting cells were rinsed in PBS and centrifuged. At this time, any contaminating red blood cells were lysed using RBC lysis buffer (Sigma) according to manufacturer's instruction, rinsed twice with PBS and passed over a 40-µm filter (Fisher Scientific). Cells were then stained for CD11b and CD45 for flow cytometry (see below). Each sorting experiment was performed on cells pooled from five mice per experiment.

Staining for CD11b and CD45 and FACS. After isolations, cell pellets were resuspended in blocking buffer (PBS/1 mM EDTA/2% donkey serum) containing 1 µg ml^{-1} Fc block (BD Pharmingen) and incubated on ice for 10 min. Cells were co-stained for 30 min on ice with Alexa 647–labeled anti-CD11b (clone M/170, Biolegend, 5 µg ml^{-1}) and Alexa 488–labeled CD45 (Biolegend, clone 30-F11, 5 µg ml^{-1}). Cells were then rinsed in PBS/EDTA centrifuged, resuspended in PBS/EDTA containing 1% fetal bovine serum and filtered into 5-ml polystyrene filter top tubes (BD Falcon) for sorting.Cells were sorted based on CD11b/CD45 expression[24] using FACS ARIA(BD). Sorted cells were centrifuged 400*g* for 10 min and pellets were either lysed in RLT-Plus buffer (Qiagen) for RNA extraction or stored at −80 °C for protein extraction and proteomics analysis.

RNA and DRS. RNA was isolated from flow cytometry–sorted cell populations using RNeasy Plus micro/mini kits (Qiagen) depending on cell number. For RNA from whole brains, 6 mice were killed, perfused with PBS/EDTA and brains were removed and homogenized in Qiazol using the TissueShredder (Qiagen) and RNA isolated with RNeasy Plus Minikit (Qiagen). Three pools of two brains per pool were created for whole brain RNA. Purified RNAs were quantified with a Nandrop 2000 (Thermo Scientific) and the quality of the RNA assessed using an Agilent Bioanalyzer (Agilent), all RNA used had an RNA Integrity Number > 9.2. RNAs from each population set were pooled as needed to yield samples containing at least 300 ng of RNA. There were three pools of microglia RNA from 22, 10, and 20 5-month-old mice, three pools of RNA from 24-month-old mice comprising 10 mice per pool, and three pools of macrophage RNA that represented 10 mice each. DRS was performed by Helicos using Helicos single molecule prototype sequencers[22,51–53]. On average 14,376,408 and 19,007,620 reads were obtained from each microglial and macrophage samples respectively. Of these, 8,480,397 reads and 11,946,274 were annotated for microglia and macrophages respectively. RNA samples that were sent to Helicos were coded such that the identity of the cell types was not known.

RNAscope. RNA scope is an RNA *in situ* hybridization technique that allows visualization of two RNA biomarkers in single cells. RNAscope uses a unique probe design strategy that results in signal amplification and background suppression[37]. RNA scope was performed at Advanced Cell Diagnostics where the technique was developed. Briefly, frozen brains from C57BL/6 mice were cut horizontally and slices were hybridized with several dual probes sets using CD11b conjugated to Alexa 546 as the common probe in each set. The companion probes to $CD11b^{Alexa546}$ were HexB, Cx3cr1, P2ry6 and P2ry12 (all conjugated to Alexa 488) and nuclei were visualized using DAPI. The resulting hybridized brain slices were imaged using the Mirax MIDI slide scanner to visualize the entire slice. To quantify cells that expressed both Cd11b and other genes of interest, CD11b-positive cells were first identified and annotated using Panoramic Viewer 1.15.2 software (3D Histech); for each brain slice, 100 cells were counted in cortex, 100 cells in the hippocampus and 50 cells in the cerebellum. The number of double-positive cells was then quantified. Each data point represents mean ± s.d. of 2–3 brain slices for each probe set. Dual RNAscope experiments were repeated twice on different slide sets with similar results.

Bioinformatics analysis. Raw reads were filtered to remove low-quality reads and those that do not meet a filter length. For each sample, Helicos provided the alignment files that also contain the query and reference sequences. Each sample alignment file was processed individually by a program written in MolBioLib[25] to determine which gene(s) (if any) were hit by each alignment. The number of hits was recorded both in raw units as well as in CMMR-normalized units[54]. Only the hits to the sense of the genes are kept. The raw counts were analyzed using EdgeR[27,55,56] to generate *P* values. EdgeR estimates the common negative binomial dispersion by conditional maximum likelihood. The $\log_2$ of the CMMR-normalized values were used as input to discover signatures for class types by using the gene expression monitoring scoring system[57]. Scores are sorted with the largest score indicating genes that are most enriched in the class in question and least enriched outside of that class. The gene set enrichment analysis was performed using the GSEA software[26,58] using the complete set of normalized input values, the c2.all.v3.0.symbols.gmt curated gene set, 1,000 gene permutations, and using the classes (for example, old versus young) as the phenotype. (The gene symbol 'chip' was selected as the chip platform.) All processing unless otherwise noted was done in the MolBioLib framework. For all statistical analysis, differences were considered statistically significant if *P* values calculated by EdgeR as well as Student *t* test were <0.05. No statistical methods were used to pre-determine sample sizes, but our sample sizes were similar to those generally employed in the field.

Proteomics. 2-D DIGE and mass spectrometry protein identification were performed by Applied Biomics. Proteomic analysis was done on microglial and macrophage lysates using pooled cells isolated from 70 mice and 50 mice, respectively.

Cell lysate preparation. Frozen cell pellets were lysed in 200 µl 2-D cell lysis buffer (30 mM Tris-HCl, pH 8.8, containing 7 M urea, 2 M thiourea and 4% CHAPS). The cells were sonicated at 4 °C, incubated on a shaker for 30 min at 22–25 °C, followed by centrifugation for 30 min at 16,000*g*. Supernatants were collected and protein concentrations determined by the Bio-Rad Protein Assay (Biorad). Sample lysates were diluted with the sample 2-D cell lysis buffer to the same protein concentration of 3 to 8 mg ml^{-1}.

Minimal CyDye labeling. To 30 µg of cell lysate, 1.0 µl of diluted CyDye (Cy2, Cy3 or Cy5) (1:5 diluted with DMF from 1 nmol $µl^{-1}$ stock) was added, incubated on ice for 30 min in the dark, followed by addition of 1.0 µl of 10 mM Lysine to each of the samples and incubation on ice in the dark for additional 15 min. Cy2, Cy3 and Cy5labeled samples were mixed together followed by addition of 2× 2-D Sample buffer (8 M urea, 4% CHAPS, 20 mg ml^{-1} DTT, 2% pharmalytes and trace amount of bromophenol blue), and loaded onto a 13-cm IPG strip.

IEF and SDS-PAGE. After loading the labeled samples into the strip holder, isoelectric focusing was run in the dark at 20 °C according to the protocol

doi:10.1038/nn.3554

provided by Amersham BioSciences. Upon finishing the IEF, the IPG strips were incubated in equilibration buffer 1 (50 mM Tris-HCl, pH 8.8, containing 6 M urea, 30% glycerol, 2% SDS, trace amount of bromophenol blue and 10 mg ml^{-1} DTT) for 15 min with slow shaking. Then the strips were rinsed in equilibration buffer 2 (50 mM Tris-HCl, pH 8.8, containing 6 M urea, 30% glycerol, 2% SDS, trace amount of bromophenol blue and 45 mg ml^{-1} iodacetamide) for 10 min with slow shaking. The IPG strips were then rinsed once in the SDS gel running buffer before being transferred to the SDS gel (12% SDS gel prepared using low florescent glass plates) and sealed with 0.5% agarose solution (wt/vol, in SDS gel running buffer). The SDS gels were run at 15 °C and until the dye front reached the end of the gel.

Image scan and data analysis. Image scans were carried out immediately following the SDS-PAGE using Typhoon TRIO (Amersham BioSciences) following the protocols provided. The scanned images were then analyzed by Image QuantTL software (GE Healthcare), and then subjected to in-gel analysis and cross-gel analysis using DeCyder software version 6.5 (GE Healthcare). The ratio change of the protein differential expression was obtained from in-gel DeCyder software analysis.

Spot picking and trypsin digestion. The spots of interest were picked up by Ettan Spot Picker (GE Healthcare) based on the in-gel analysis and spot picking design by DeCyder software. The gel spots were washed, followed by in-gel digestion with modified porcine trypsin protease (Trypsin Gold, Promega). The digested tryptic peptides were desalted by Zip-tip C18 (Millipore). Peptides were eluted from the Zip-tip with 0.5 µl of matrix solution (α-cyano-4-hydroxycinnamic acid, 5 mg ml^{-1} in 50% acetonitrile, 0.1% trifluoroacetic acid, 25 mM ammonium bicarbonate) and spotted on the MALDI plate.

Mass spectrometry. MALDI-TOF (MS) and TOF/TOF (tandem MS/MS) were performed on a 5800 mass spectrometer (AB Sciex). MALDI-TOF mass spectra were acquired in reflectron positive ion mode, averaging 2,000 laser shots per spectrum. TOF/TOF tandem MS fragmentation spectra were acquired for each sample, averaging 2,000 laser shots per fragmentation spectrum on each of the 5–10 most abundant ions present in each sample (excluding trypsin autolytic peptides and other known background ions).

Database search. Both the resulting peptide mass and the associated fragmentation spectra were submitted to GPS Explorer version 3.5 equipped with MASCOT search engine (Matrix science) to search the database of National Center for Biotechnology Information non-redundant. Searches were performed without constraining protein molecular weight or isoelectric point, with variable carbamidomethylation of cysteine and oxidation of methionine residues, and with one missed cleavage allowed in the search parameters. Candidates with either protein score confidence interval percent or Ion confidence interval percent greater than 95 were considered significant.

Quantitative real-time PCR. Microglia and peritoneal macrophages were isolated from a different cohort of 5-month-old mice than the ones used for DRS comprising 6 sets of 5 mice per set. The sorts resulted in 6 pools of macrophages and 5 pools of microglia. Total RNA from each sample of cells ($3.0–8.0 \times 10^5$ cells) was isolated using the RNeasy Plus micro kit (Qiagen) according to the manufacturer's instructions and reverse transcribed using Multiscribe reverse transcriptase (Applied Biosystems). Dilutions of each cDNA prep were used to assess β2-microglobulin RNA levels and samples were then adjusted to give equivalent levels of β2-microglobulin per well in subsequent qPCR reactions for other genes. The qPCR was performed in a Roche 480 Lightcycler qPCR machine in duplicates using SYBR Green to detect the amplification products. The following cycles were performed: initial denaturation cycle 95 °C for 10 min, followed by 40 amplification cycles of 95 °C for 15 s and 60 °C for one min and ending with one cycle at 25 °C for 15 s. Relative quantification of mRNA expression was calculated by the comparative cycle method to obtain the ratio of gene interest/B2M.

The following genes and primers were used: *Cd11b* (GTGTGACTA CAGCACAAGCCG, CCCAAGGACATATTCACAGCCT), *Cx3cr1* (ACCGGT ACCTTGCCATCGT, ACACCGTGCTGCACTGTCC), *Hexb* (ACTCCAAGATTA TGGCCTCGAGCA, GCTATTCCACGGCTGACCATTCT), *B2M* (CCGAAC ATACTGAACTGCTACG, CCCGTTCTTCAGCATTTGGA), *P2ry6* (CTGC GTCTACCGTGAGGATT, GCAATGACGCAGATGTTCAG), *P2ry12* (CACGG ATTCCCTACACCCTG, GGGTGCTCTCCTTCACGTAG), *P2ry13* (AACAAA GCTGATGCTCGGGA, GTGTCATCCGAGTGTCCCTG), *Trem2* (GCCTTCCT GAAGAAGCGGAA, GAGTGATGGTGACGGTTCCA).

51. Ozsolak, F. *et al.* Digital transcriptome profiling from attomole-level RNA samples. *Genome Res.* **20**, 519–525 (2010).
52. Ozsolak, F. & Milos, P.M. RNA sequencing: advances, challenges and opportunities. *Nat. Rev. Genet.* **12**, 87–98 (2011).
53. Ozsolak, F. *et al.* Amplification-free digital gene expression profiling from minute cell quantities. *Nat. Methods* **7**, 619–621 (2010).
54. Mortazavi, A., Williams, B.A., McCue, K., Schaeffer, L. & Wold, B. Mapping and quantifying mammalian transcriptomes by RNA-Seq. *Nat. Methods* **5**, 621–628 (2008).
55. Robinson, M.D. & Smyth, G.K. Moderated statistical tests for assessing differences in tag abundance. *Bioinformatics* **23**, 2881–2887 (2007).
56. Robinson, M.D. & Smyth, G.K. Small-sample estimation of negative binomial dispersion, with applications to SAGE data. *Biostatistics* **9**, 321–332 (2008).
57. Golub, T.R. *et al.* Molecular classification of cancer: class discovery and class prediction by gene expression monitoring. *Science* **286**, 531–537 (1999).
58. Mootha, V.K. *et al.* PGC-1alpha-responsive genes involved in oxidative phosphorylation are coordinately downregulated in human diabetes. *Nat. Genet.* **34**, 267–273 (2003).